

PERFORMANCE-BASED SEISMIC DESIGN OF NON-EMULATIVE PRECAST CONCRETE WALLS WITH FRICTION DAMPERS

Yahya C. KURAMA¹

ABSTRACT

Precast concrete structures in seismic regions have been traditionally designed to emulate the behavior of monolithic cast-in-place concrete structures largely because of limited knowledge about their seismic behavior. In recent years, a significant amount of research has been conducted on precast walls which do not emulate monolithic cast-in-place concrete walls because of their economy, construction simplicity, and desirable seismic characteristics such as a self-centering capability and an ability to undergo “large” nonlinear lateral displacements with little damage. The greatest disadvantage of non-emulative precast walls in seismic regions is an increase in the lateral displacements as a result of small inelastic energy dissipation. It is possible to reduce these displacements by using friction dampers along vertical joints between the walls, without losing the desirable characteristics of the walls. The paper introduces a performance-based seismic design approach to reduce the maximum lateral displacements of the walls below a target displacement using supplemental friction dampers. Nonlinear dynamic analyses of prototype walls with different fundamental periods of vibration show that the design approach is effective in reducing the lateral displacements to prevent significant damage in the walls under severe ground motions.

1. INTRODUCTION AND BACKGROUND

Recent research conducted as a part of the PREcast Seismic Structural Systems (PRESSS) Program (Kurama et al. 1999; Priestley et al. 1999) has shown that the use of unbonded post-tensioning in non-emulative precast concrete walls results in desirable seismic characteristics such as a self-centering capability and an ability to undergo “large” lateral displacements with little damage. The greatest disadvantage of these walls in seismic regions is an increase in the lateral displacements as a result of small inelastic energy dissipation (Kurama 2000). Perez (1999) and Priestley et al. (1999) investigated the use of metallic yield dampers along vertical joints between precast walls to reduce the lateral displacements under ground motions. The use of supplemental viscous fluid-dampers to reduce the displacements of the walls was investigated by Kurama (2000).

This paper addresses the seismic behavior and design of unbonded post-tensioned precast walls with supplemental friction dampers along vertical joints. Fig. 1(a) shows the plan layout of a

¹ Civil Engineering and Geological Sciences, University of Notre Dame, Notre Dame, IN 46556, U.S.A.
E-mail: Kurama.1@nd.edu

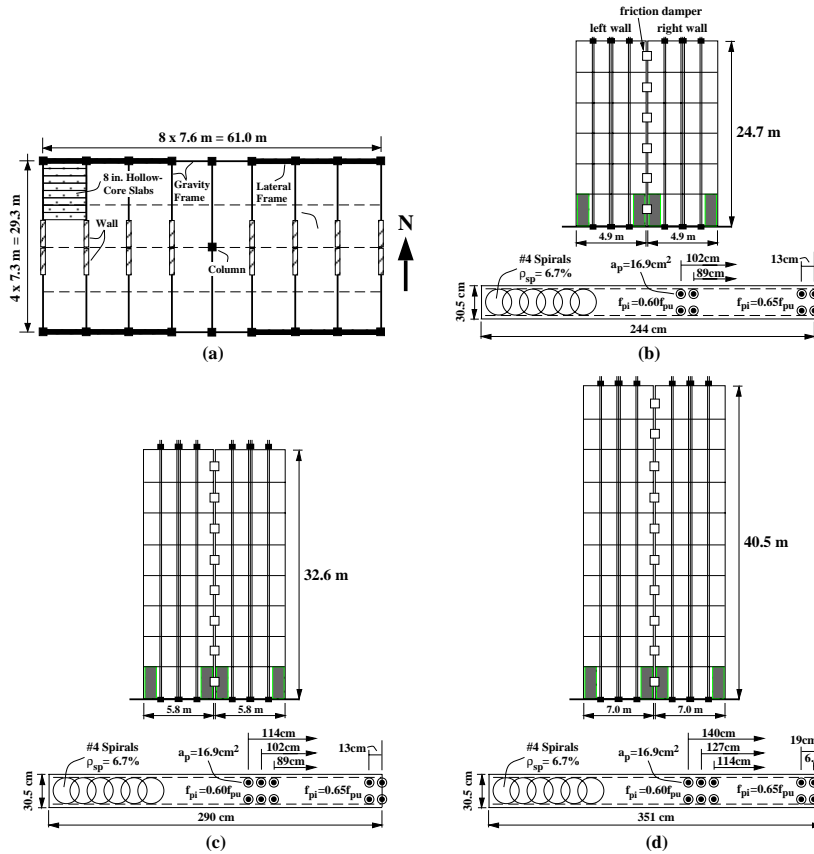


FIG. 1. Prototype buildings: (a) plan layout; (b) Wall CW1; (c) Wall CW2; (d) Wall CW3

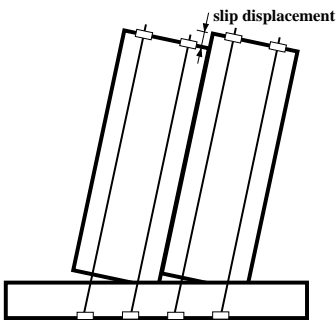


FIG. 2. Idealized slip displacements

the horizontal joints as shown in Fig. 2. It is noted that only the gap opening along the base-panel-to-foundation joint is shown in the idealized displaced shape of the wall in Fig. 2. In an actual wall, the slip displacements vary along the height of the wall as a result of the deformations of the wall, including gap opening along the upper story horizontal joints. Recent tests of precast walls with metallic yield dampers along vertical joints at the University of California at

San Diego (Priestley et al. 1999) have demonstrated that gap opening and slip displacements similar to Fig. 2 can occur without damaging the floor system.

Fig. 3(a) shows the expected base-shear-roof-displacement ($V-u$) behavior of Wall CW1 without the friction dampers under combined gravity loads and cyclic lateral loads. The distribution of the lateral forces over the height of the wall is the same as the distribution of inertial forces corresponding to the first mode of vibration from a linear-elastic modal analysis of the structure.

prototype precast concrete office building in a region with high seismicity and a site with a medium soil profile. Figs. 1(b)-(d) show three prototype walls (Walls CW1, CW2, and CW3 with 6, 8, and 10 stories, respectively) which were designed for the building layout in Fig. 1(a).

The supplemental energy dissipation system uses the relative slip displacements which occur along the vertical joint between the walls as a result of gap opening along

Fig. 3(a) shows that the hysteretic behavior of the wall is nearly nonlinear-elastic, characterized by loading and unloading curves that are very close to each other. The nonlinear behavior occurs primarily due to the opening of gaps along the horizontal joints (Kurama et al. 2000). The narrow hysteresis loops show that the inelastic energy dissipation of the wall is very small.

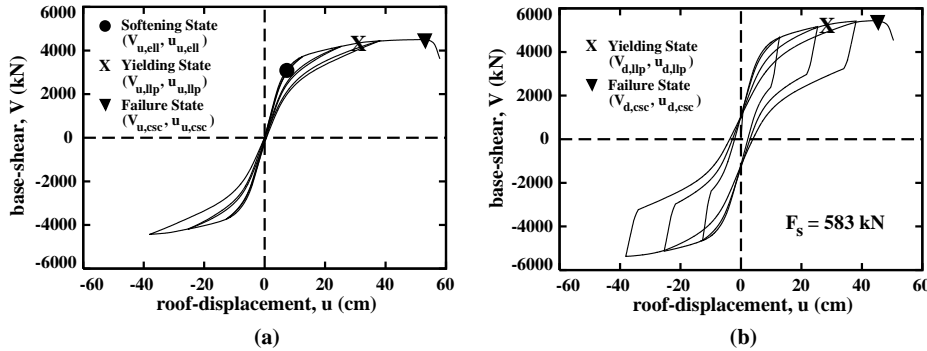


FIG. 3. Base-shear-roof-displacement relationship: (a) without dampers; (b) with dampers

Fig. 3(b) shows the expected V-u behavior of Wall CW1 with friction dampers. The slip force for the dampers, F_s is assumed to be equal to 583 kN. The results show that the inelastic

energy dissipation capacity of the wall is significantly increased by the friction dampers as indicated by the much fuller hysteresis loops in Fig. 3(b). The self-centering capability of the wall (i.e., the ability of the wall to return towards its undisplaced position upon unloading from a large nonlinear displacement) is preserved.

Figs. 3(a) and (b) indicate that the lateral displacements of unbonded post-tensioned walls can be reduced by using friction dampers. A design approach for the walls without the dampers is described in Kurama et al. (1999). This paper proposes a performance-based seismic design approach for the dampers to reduce the maximum roof displacements below a target roof displacement to prevent significant damage in the walls. The adequacy of the design approach is evaluated based on nonlinear dynamic time-history analyses of Walls CW1, CW2, and CW3.

2. ANALYTICAL MODEL

Fig. 4(a) shows the analytical model for Wall CW1. The analytical modeling of walls without dampers is discussed by Kurama et al. (1999) and is not described here in detail. Fiber beam-column elements are used to model the concrete wall panels and truss elements are used to model the unbonded post-tensioning steel. The model, which is referred to as the fiber wall model,

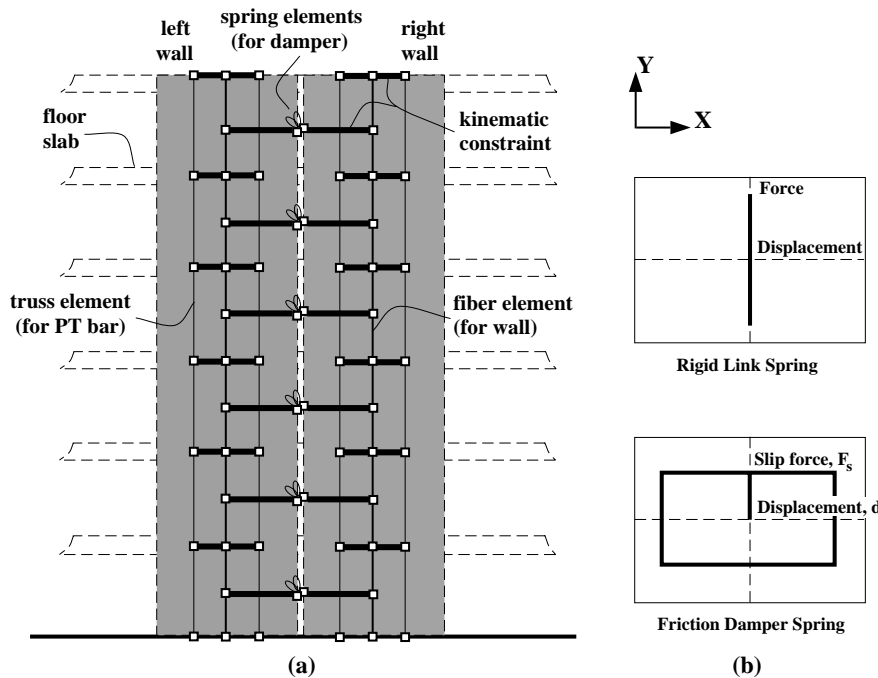


Fig. 4. Wall model: (a) multi-story wall; (b) spring elements

accounts for axial-flexural interaction, hysteretic behavior of the post-tensioning steel and concrete including concrete crushing, and gap opening along the horizontal joints. The verification of the fiber wall model is described in Kurama (2000).

The friction dampers are modeled using zero-length spring elements as shown in

Fig. 4(a). The X-displacement, Y-displacement, and rotation degrees-of-freedom (DOF) of the damper nodes are kinematically constrained to the DOF of the corresponding wall nodes (at the same height as the damper nodes). Two zero-length spring elements are used between each pair of damper nodes. Fig. 4(b) shows the hysteretic force-displacement relationships of the spring elements. The first spring element is a rigid link element in the X-direction in order to ensure that the two walls go through the same lateral displacements. The second spring element is defined in the Y-direction to represent the behavior of the friction dampers along the vertical joint between the walls. The friction mechanism is characterized by close-to rectangular hysteresis loops, which are assumed to be generated by Coulomb friction. It is assumed that the anchorages between the walls and the dampers are properly designed for the maximum damper forces.

3. GROUND MOTION RECORDS

Two sets of ground motion records are used which are representative of maximum credible ground motions that can be expected in regions of the U.S. with high seismicity. The first set includes seven ground motions (five natural records and two generated records) selected and scaled at the University of Notre Dame as described in Kurama (2000). The Notre Dame (ND)

ground motions are scaled to a constant maximum incremental velocity, MIV of 171 cm/sec. The MIV of a ground motion is equal to the maximum area under the acceleration time-history of the ground motion between two successive zero acceleration crossings. The ground motions are for sites with a medium soil profile similar to the site soil condition used in the design of the prototype walls. The second set includes twenty ground motion records (ground motions LA21 through LA40), having probabilities of exceedence of 2% in 50 years, as compiled and scaled by the SAC steel project (Somerville 1997).

4. SDOF REPRESENTATION OF THE UNDAMPED WALL SYSTEM

The seismic design of the friction dampers is based on a single-degree-of-freedom (SDOF) representation of the multi-degree-of-freedom (MDOF) wall system. For this purpose, the wall without the friction dampers is referred to as the “undamped” wall, which is assumed to have a viscous damping ratio of 3% in the first and third modes (using Rayleigh damping). The properties of the SDOF system are determined based on the linear-elastic first (i.e., fundamental) mode response of the MDOF system. The linear-elastic frequency and damping ratio of the SDOF system are assumed to be equal to the linear-elastic first mode circular frequency, ω_u and viscous damping ratio, ξ_u of the undamped MDOF system, respectively.

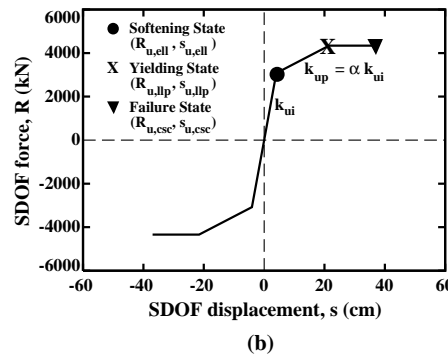
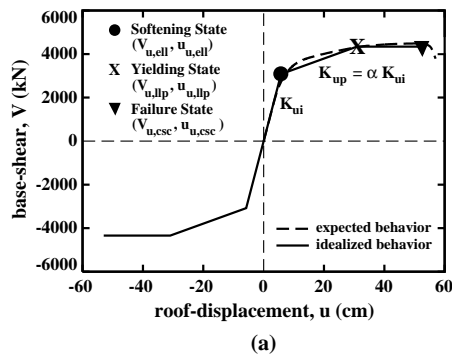


FIG. 5. SDOF representation of the undamped wall: (a) idealized MDOF model; (b) SDOF model

The nonlinear force-displacement (R-s) relationship of the SDOF system is determined as follows. Fig. 5(a) shows a trilinear idealization of the V-u relationship of

Wall CW1 (without the dampers) in Fig. 3(a). The trilinear idealization of the V-u relationship is based on (Kurama et al. 1999): (1) the “softening” state (indicated by a ● marker) which identifies the beginning of a significant reduction in the lateral stiffness of the wall due to gap opening along the horizontal joints and nonlinear behavior of the concrete in compression (at a

base shear and roof displacement of V_{ell} and u_{ell} , respectively); (2) the “yielding” state (indicated by a **X** marker) which identifies the point at which the strain in the post-tensioning steel reaches the limit of proportionality for the first time (at V_{llp} and u_{llp}); and (3) the “failure” state (indicated by a **▼** marker) which identifies axial-flexural failure of the wall as a result of crushing of the spiral confined concrete (Fig. 1) near the base (at V_{csc} and u_{csc}). Note that the subscripts u and d in Figs. 3(a) and (b) refer to walls without and with dampers, respectively.

Fig. 5(b) shows the nonlinear force-displacement (R-s) relationship of the SDOF system to represent the idealized V-u relationship of the undamped MDOF system in Fig. 5(a). The SDOF displacements, s are determined by dividing the MDOF roof displacements, u with the roof displacement participation factor, Γ based on the first linear-elastic mode shape of the wall as

$$\begin{aligned}
 s_{u,ell} &= \frac{u_{u,ell}}{\Gamma} \\
 s_{u,llp} &= \frac{u_{u,llp}}{\Gamma} \\
 \Gamma &= \frac{L}{M^*} \\
 L &= \{ \phi_{u1} \}^T [M] \{ 1 \} \\
 M^* &= \{ \phi_{u1} \}^T [M] \{ \phi_{u1} \}
 \end{aligned} \tag{1}$$

where L is the earthquake excitation factor and M^* is the generalized mass for the first mode, $\{ \phi_{u1} \}$ is the first linear-elastic mode-shape of the undamped wall normalized with respect to the roof, and $[M]$ is the diagonal mass matrix assigned to the wall. The mass of the SDOF system is assumed to be equal to the effective first mode mass, m of the MDOF system as $m=L^2/M^*$ and, the initial stiffness, k_{ui} and post-softening stiffness, k_{up} of the SDOF system are calculated as

$$\begin{aligned}
 k_{ui} &= m \omega_u^2 \\
 k_{up} &= \alpha k_{ui} \\
 \alpha &= \frac{V_{u,llp}/V_{u,ell} - 1}{u_{u,llp}/u_{u,ell} - 1}
 \end{aligned} \tag{2}$$

where α is the post-softening stiffness ratio of the undamped MDOF wall system. The hysteretic force-displacement relationship of the SDOF system in Fig. 5(b) is assumed to be nonlinear-elastic (i.e., with no inelastic energy dissipation). Thus, the small amount of inelastic energy dissipation of the MDOF system in Fig. 3(a) is ignored.

5. SDOF REPRESENTATION OF THE DAMPED WALL SYSTEM

Fig. 6(a) shows the shear forces and axial forces that develop at the base of the left wall and right wall as a result of the coupling that occurs between the two walls due to the damper forces. The coupling base shear, V_s and roof displacement, u_s corresponding to the slip of the dampers can be calculated as

$$\begin{aligned} V_s &= \frac{n_d F_s l_w}{\bar{h}} \\ u_s &= \frac{V_s}{K_s} = \frac{V_s}{K_{di} - K_{ui}} \end{aligned} \quad (3)$$

where n_d is the number of dampers, F_s is the slip force for one damper, l_w is the length of one wall, \bar{h} is the resultant height of first mode inertia forces, K_s is the increase in the initial lateral stiffness of the wall system due to the coupling between the walls, and K_{di} and K_{ui} are the initial lateral stiffness of the damped and undamped systems, respectively. It is assumed that all dampers slip at the same roof displacement.

Fig. 6(b) shows the coupling base-shear-roof-displacement relationship of the walls due to the damper forces. The SDOF representation of the coupling base-shear-roof-displacement relationship is shown in Fig. 6(c). The initial stiffness, k_s and slip displacement, s_s for the SDOF damper model in Fig. 6(c) are

$$\begin{aligned} k_s &= k_{di} - k_{ui} = m \omega_u^2 \left(\frac{\omega_d^2}{\omega_u^2} - 1 \right) \\ s_s &= u_s / \Gamma \end{aligned} \quad (4)$$

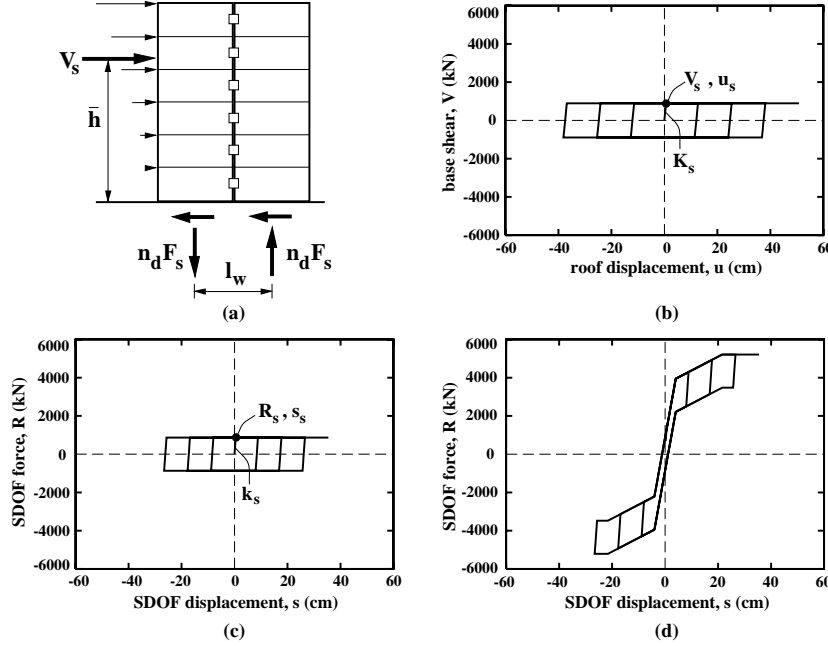


FIG. 6. SDOF representation of the damped wall: (a) coupling forces; (b) MDOF damper model; (c) SDOF damper model; (d) SDOF wall model

undamped system. The resulting SDOF force-displacement (R - s) relationship for the damped wall system is obtained by superposing the relationships in Figs. 5(b) and 6(c) as shown in Fig. 6(d).

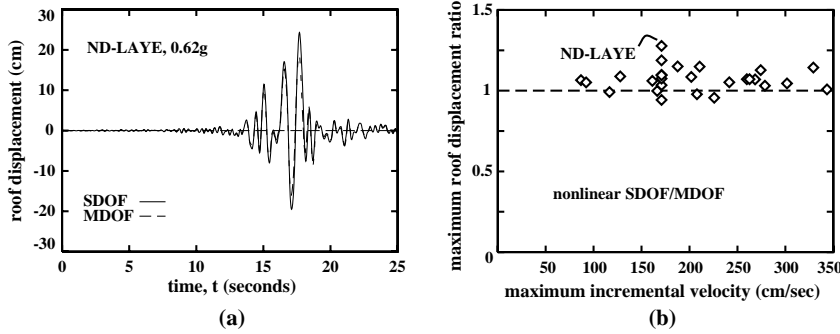


FIG. 7. Nonlinear SDOF model: (a) displacement time-history; (b) maximum displacement ratio

displacements of the SDOF system are multiplied with the roof displacement participation factor, Γ . Fig. 7(b) shows the ratio between the maximum displacements of the SDOF system and the damped MDOF system under the 27 ND and SAC ground motions. On average, the ratio between the maximum displacements of the SDOF and MDOF systems is equal to 1.07.

It is concluded that the nonlinear SDOF system is capable of predicting both the maximum displacement and the roof-displacement time-history of the damped MDOF wall system

where ω_d is the linear-elastic first mode circular frequency of the damped MDOF system. It is noted that the linear-elastic first mode shape of the undamped system is used in the determination of \bar{h} , m , and Γ in Eqs. (3) and (4) since slip of the dampers occurs very early in the response, and thus, the response of the damped wall system is primarily governed by the mode shapes of the

undamped system. The resulting SDOF force-displacement (R - s) relationship for the damped wall system is obtained by superposing the relationships in Figs. 5(b) and 6(c) as shown in Fig. 6(d). Fig. 7(a) compares the roof-displacement time-history of the damped MDOF system in Fig. 3(b) (using the fiber wall model) and the SDOF system in Fig. 6(d) under the ND Landers-Yermo (LAYE) ground motion. It is noted that the

reasonably well. The maximum displacement of the SDOF system is usually slightly larger than that of the MDOF system because of the small amount of inelastic energy dissipated by the undamped system (as shown in Fig. 3(a)) which is ignored in the SDOF system.

6. EQUIVALENT LINEARIZATION OF THE SDOF SYSTEM

For the SDOF system exhibiting the nonlinear properties in Fig. 6(d), the maximum displacement response can be reasonably approximated using an equivalent linear-elastic SDOF system whose stiffness and damping properties are expressed in terms of the properties of the nonlinear system as follows. Iwan and Gates (1979) have proposed an average stiffness method to determine the equivalent linear-elastic stiffness to represent a bilinear elasto-plastic system. This method is extended here to the trilinear undamped SDOF system shown in Fig. 5(b). It is noted that the increase in the initial stiffness of the wall due to the dampers is neglected since slip of the dampers occurs very early in the response. Thus, the equivalent linear-elastic stiffness is determined based on the undamped SDOF system only. According to the average stiffness method, the equivalent linear-elastic stiffness, k_e is calculated as

$$k_e = \frac{1}{s_{\max}} \int_0^{s_{\max}} k_u(s) ds \quad (5)$$

$$k_e = k_{ui} e_k$$

which, for the trilinear system in Fig. 5(b), results in

$$\begin{aligned} (s_{u,ell} \leq s_{\max} \leq s_{u,llp}) &\Rightarrow e_k = (1-\alpha) \frac{1 + \ln(s_{\max}/s_{u,ell})}{s_{\max}/s_{u,ell}} + \alpha \\ (s_{\max} > s_{u,llp}) &\Rightarrow e_k = (1-\alpha) \frac{1 + \ln(s_{\max}/s_{u,ell})}{s_{\max}/s_{u,ell}} + \alpha \frac{1 + \ln(s_{\max}/s_{u,llp})}{s_{\max}/s_{u,llp}} \end{aligned} \quad (6)$$

where s_{\max} is the maximum displacement, $s_{u,ell}$ and $s_{u,llp}$ are defined in Eq. (1), and k_{ui} and α are defined in Eq. (2).

The equivalent viscous damping ratio of the linear-elastic system is determined using a variation of the Resonant Amplitude Matching method (Iwan and Gates 1979) as

$$\xi_e = \frac{D_h}{2 \pi k_e s_{\max}^2} + \xi_u \sqrt{\frac{1}{e_k}} \quad (7)$$

$$D_h = 4 k_s s_s (s_{\max} - s_s)$$

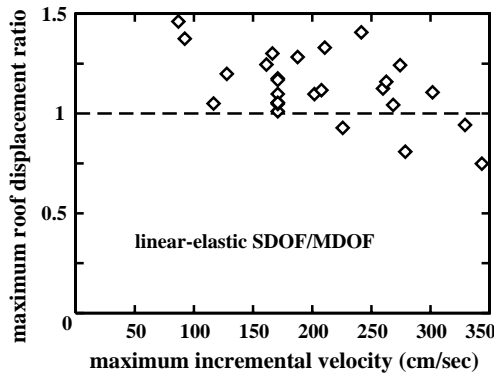


FIG. 8. Equivalent linear SDOF model

where D_h is the energy dissipated by the SDOF damper model in Fig. 6(c) during one cycle of response to the maximum displacement (i.e., between s_{\max} and $-s_{\max}$). The shift in the frequency of the nonlinear system is included in the estimation of ξ_e as indicated by the use of k_e in Eq. (7).

Fig. 8 shows the ratio between the maximum displacements of the linear-elastic SDOF system and the nonlinear MDOF system under the 27 ground motions. On average, the ratio between the maximum displacements of the two systems is equal to 1.13.

7. DESIGN APPROACH

This section describes the design of the supplemental friction dampers along the vertical joints. The seismic design of the walls without the friction dampers is discussed in Kurama et al. (1999) and is not described here. The objective of the design approach is to determine the required damper slip force to reduce the maximum roof-displacement of the walls below a target roof-displacement. This is achieved by comparing the capacity of the walls in the form of an effective “capacity curve” with equivalent seismic demands in the form of average ground motion “demand spectra” as described in Kurama (2000). The design approach is demonstrated below using Wall CW1.

7.1 Ground motion demand spectra and structure capacity curve

The demand spectra for a ground motion are constructed by plotting the linear-elastic SDOF pseudo-acceleration response spectra, S_a versus the displacement response spectra, S_d for different values of the viscous damping ratio, ξ . In the design of the dampers for the prototype walls, average demand spectra using the seven MIV-scaled ND ground motions were used. The thin

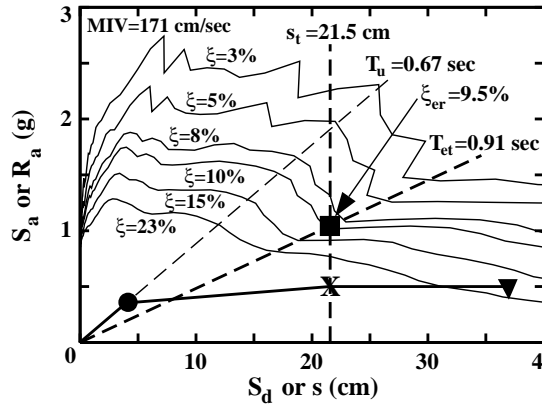


FIG. 9. Design approach

solid lines in Fig. 9 show the average demand spectra (normalized with respect to g) of the ND ground motions for damping ratios of $\xi = 3, 5, 8, 10, 15,$ and 23% , respectively.

The capacity curve is determined from the nonlinear SDOF force-displacement (R - s) relationship of the undamped wall in Fig. 5(b). The SDOF force, R is converted to an effective SDOF acceleration, R_a by dividing with the effective first mode mass as $R_a = R/m$. The capacity curve for Wall CW1 is shown by the heavy solid line in Fig. 9. The light dashed radial line corresponds to the linear-elastic fundamental period of the undamped wall, $T_u = 2\pi/\omega_u = 0.67$ sec.

7.2 Target roof-displacement and equivalent fundamental period

As stated above, the objective of the design approach is to determine the required slip force of the dampers to reduce the maximum roof-displacement of the wall below a target roof-displacement, u_t . In order to prevent significant damage in the walls (Kurama 2000), the dampers are designed for a target roof-displacement of $u_t = u_{u,llp}$ (corresponding to the yielding state). The vertical dashed line in Fig. 9 shows the target roof-displacement for Wall CW1, $u_t = u_{u,llp} = 30.9$ cm converted to the target SDOF displacement, $s_t = s_{u,llp} = u_{u,llp} / \Gamma = 21.5$ cm.

The heavy dashed radial line in Fig. 9 represents the equivalent fundamental period, T_{et} for the wall corresponding to the target displacement, u_t as $T_{et} = 2\pi(m/k_{et})^{0.5}$ where k_{et} is the equivalent stiffness of the wall corresponding to the target displacement, u_t . For $u_t = u_{u,llp}$, T_{et} is estimated as 0.91 sec. using Eqs. (5) and (6) with $s_{max} = s_t = 21.5$ cm. The estimated T_{et} represents a 35% elongation over the initial linear-elastic fundamental period of the undamped wall, $T_u = 0.67$ sec.

7.3 Required equivalent viscous damping ratio and damper slip force

The equivalent fundamental period T_{et} is used together with the capacity curve and the average demand spectra in Fig. 9 to estimate the required equivalent viscous damping ratio, ξ_{er} . The intersection point between the vertical line (at $s_t = 21.5$ cm) and the heavy radial line (at $T_{et} = 0.91$ sec.) gives the required equivalent viscous damping ratio, ξ_{er} to reduce the maximum roof-displacement below the target displacement. The estimated ξ_{er} for Wall CW1 is equal to 9.5%.

The required damper slip force, F_{sr} to achieve the damping ratio, ξ_{er} is estimated for an assumed number of dampers, n_d using Eqs. (3), (4), and (7). It is assumed that the dampers have the same slip force. For preliminary design $K_{di} / K_{ui} \approx (n_w l_w)^3 / n_w l_w^3 = n_w^2$, where $n_w = 2$ is the number of walls may be used assuming that the dampers provide full coupling between the walls until slip occurs. Assuming that the system without the dampers has a viscous damping ratio of $\xi_u = 3\%$, the estimated required damper slip force for Wall CW1 is $F_{sr} = 537$ kN with $n_d = 6$ (Fig. 1(b)).

8. EVALUATION OF DYNAMIC RESPONSE

The proposed design approach for the friction dampers is evaluated based on nonlinear dynamic time-history analyses of Walls CW1, CW2, and CW3. The walls without the dampers (Table 1) were designed for a region with high seismicity and a site with a medium soil profile (site class D as defined in NEHRP-97 (FEMA 1998)) using a seismic design approach described in Kurama et al. (1999) and the provisions of NEHRP-97. In Table 1, the roof-displacements of the walls, u are given in terms of the roof-drift, Δ (%) by dividing the displacements with the wall height.

The friction dampers for the walls were designed as demonstrated above for Wall CW1. The estimated equivalent fundamental period, T_{et} , required equivalent viscous damping ratio, ξ_{er} , and required damper slip force, F_{sr} for the walls corresponding to the target roof-drift, $\Delta_t = \Delta_{u,lp}$ at the yielding state are given in Table 2.

Figs. 10(a)-(c) show the maximum roof-drift, Δ_{max} from the dynamic analyses of the walls. The dynamic analyses were conducted using the fiber wall model under the seven MIV-scaled ND ground motions, and with a time step of 0.01 sec. Table 3 shows the average maximum roof-

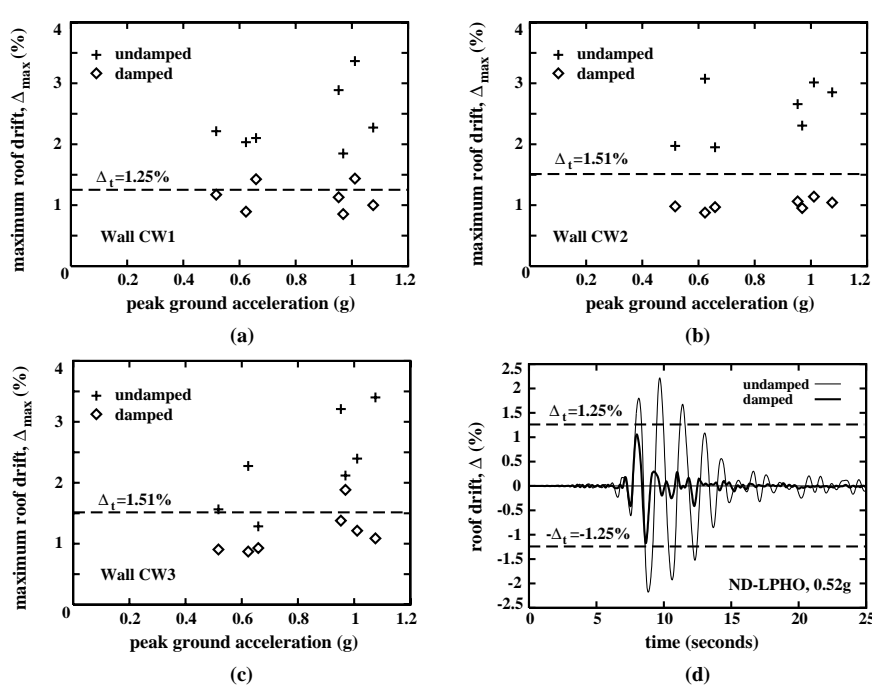


FIG. 10. Evaluation of dynamic response: (a)-(c) maximum roof-drift of Walls CW1, CW2, CW3, respectively; (d) roof-drift time-history for Wall CW1

The dynamic analysis results indicate that the supplemental energy dissipation system is, on average, effective in significantly reducing the maximum roof-drift of the walls. The average ratio between the maximum roof-drift of the damped walls and undamped walls are equal to 0.48, 0.41, and 0.55 for Walls CW1, CW2, and CW3, respectively. Figs. 10(a)-(c) also show that the scatter in the maximum roof-drift of the undamped walls is significantly larger than that of the damped walls.

Fig. 10(d) compares the roof-drift time-histories of Wall CW1 with and without the dampers under the MIV-scaled ND Loma Prieta-Hollister (LPHO) ground motion. The time-history results indicate that the dampers are very effective in reducing the large roof-drift cycles that occur in the undamped wall after the maximum roof-drift is reached.

The average ratio between the maximum roof-acceleration of the damped walls and undamped walls are equal to 0.83, 1.00, and 0.89 for Walls CW1, CW2, and CW3, respectively.

Table 1 - Properties of the undamped walls.

Wall	h_w (m)	l_w (m)	T_u (sec.)	$V_{u,ell}$ (kN)	$\Delta_{u,ell}$ (%)	$V_{u,llp}$ (kN)	$\Delta_{u,llp}$ (%)	$\Delta_{u,esc}$ (%)
CW1	24.7	2x4.9	0.67	3078	0.23	4342	1.25	2.15
CW2	32.6	2x5.8	0.90	3459	0.27	5041	1.51	2.26
CW3	40.5	2x7.0	1.05	4067	0.27	5799	1.51	2.78

drift, $\bar{\Delta}_{\max}$ and the average maximum roof-acceleration, \bar{a}_{\max} of the walls from the dynamic analyses. The average maximum roof-drift, $\bar{\Delta}_{\max}$ for the damped walls (i.e., with the friction dampers) are smaller than the corresponding target roof-drift, $\Delta_{u,llp}$ values in Table 2. Thus, the design objectives are on average achieved.

The dynamic analysis results

Table 2 - Damper design.

Wall	T_{et} (sec.)	ξ_{er} (%)	F_{sr} (kN)
CW1	0.91	9.6	537
CW2	1.23	12.0	733
CW3	1.43	10.6	567

Table 3 - Dynamic response of the prototype walls.

Wall	$\bar{\Delta}_{max}$ (%)		\bar{a}_{max} (g)	
	undamped	damped	undamped	damped
CW1	2.39	1.13	1.62	1.32
CW2	2.55	1.00	1.51	1.49
CW3	2.32	1.18	1.81	1.59

9. CONCLUSIONS

The paper proposes a seismic design approach for unbonded post-tensioned precast walls with friction dampers along vertical joints. The adequacy of the design approach is evaluated based on nonlinear dynamic time-history analyses of three prototype walls with and without friction dampers. The main contributions and conclusions of the paper are as follows.

1. The objective of the design approach is to determine the required damper slip force to reduce the maximum roof-displacement below an allowable target roof-displacement to prevent significant damage in the walls. This is achieved by comparing the capacity of the walls in the form of a “capacity curve” with equivalent seismic demands in the form of ground motion “demand spectra”.

2. The design approach uses an equivalent linear-elastic SDOF representation of the walls with the dampers. A method to estimate the equivalent linear-elastic SDOF stiffness and damping properties for the walls is described in the paper. As future research, it is recommended that the use of other linearization methods to represent the hysteretic force-displacement relationship of the walls is investigated.

3. Nonlinear dynamic time-history analyses of 6, 8, and 10-story prototype walls with and without friction dampers show that the proposed design approach is, on average, very effective in reducing the maximum roof-displacement below the target roof-displacement.

4. Walls with friction dampers have significantly smaller scatter in maximum roof-displacement than walls without friction dampers. Furthermore, the large roof-displacement cycles that occur in the undamped walls are significantly reduced by the friction dampers. The self-centering capability of the walls is preserved.

10. ACKNOWLEDGMENTS

The investigation is funded by the National Science Foundation (NSF) under Grant No. CMS 98-74872 as a part of the CAREER Program. The support of the NSF Program Director Dr. S. C. Liu is gratefully acknowledged. The opinions, findings, and conclusions are those of the author and do not necessarily reflect the views of the NSF or those acknowledged above.

11. REFERENCES

FEMA (1998). NEHRP recommended provisions for seismic regulations for new buildings and other structures. FEMA 302, Federal Emergency Management Agency, Washington, D.C.

Iwan, W. and Gates N. (1979). Estimating earthquake response of simple hysteretic structures. *Journal of Engineering Mechanics*, Amer. Soc. of Civil Eng., Vol. 105, No. EM3, pp. 391-405.

Kurama, Y. (2000). Seismic design of unbonded post-tensioned precast walls with supplemental viscous damping. *ACI Structural Journal*, American Concrete Institute, Vol. 97-4.

Kurama, Y., Pessiki, S., Sause, R., and Lu, L.W. (1999). Seismic behavior and design of unbonded post-tensioned precast concrete walls. *PCI Journal*, Pre./Prest. Conc. Inst., Vol. 44-3.

Perez, F. (1998). Lateral load behavior of precast concrete walls with ductile vertical joint connectors. M.S. Thesis, Dept. of Civil and Env. Engineering, Lehigh University, Bethlehem, PA.

Priestley, M., Sritharan, S., Conley, J., and Pampanin, S. (1999). Preliminary results and conclusions from the PRESSS five-story precast concrete test building. *PCI Journal*, Vol. 44-6.

Somerville, P. (1997). Development of ground motion time histories for phase 2 of the FEMA/SAC steel project. Report No. SAC/BD-97/04, SAC Joint Venture, Sacramento, CA.

12. KEYWORDS

Concrete, friction dampers, friction damping, precast concrete, precast wall, prestressed concrete, seismic design, shear wall, structural wall, supplemental damping, supplemental energy dissipation, unbonded post-tensioning.